Precision Engineering 72 (2021) 878–890

Contents lists available at ScienceDirect

Precision Engineering

journal homepage: www.elsevier.com/locate/precision

Tension management in cable transmission systems for remote manipulators

Shorya Awtar *, Adam Kim, Ashwin Thombre

Precision Systems Design Lab, Mechanical Engineering, University of Michigan, 2350 Hayward Street, Ann Arbor, MI, 48109, USA

ARTICLE INFO

Keywords:
Cable transmission
Tension management
Remote articulating manipulators

ABSTRACT

This paper presents the design of a novel kinematic tensioning system to remedy the situation where the input-output relation in the cable transmission for a remotely operated multi-link end-effector is compromised due to the onset of slack. The actuation of multi-link end-effectors in remote manipulators via cable transmission exhibits loss of tension and slack generation on the non-driving side of the cable transmission. This paper outlines an analytical formulation of the kinematic component of slack resulting from the geometry of the end-effector links that are serially connected. If left unaddressed, cable slack adversely impacts transmission stiffness and produces backlash at the end-effector wherein for a fixed input, the output can move freely over a range of motion (i.e. dead-band). In case of articulating instruments for minimally invasive surgery, this limits the ability to position and orient the end-effector precisely, the ability to effectively transmit forces via the end-effectors to the surrounding tissues, and the tactile feedback to the user operating the instrument. To overcome these limitations, this paper presents a simple solution that effectively mitigates slack on the non-driving side of a cable transmission between a driving pulley and a multi-link end-effector with minimal cost or complexity. The proposed design uses a driving pulley modified with tensioner extensions to alter the transmission path, which provides a kinematic or geometric solution in contrast to the various spring based solutions that have several drawbacks. Based on a derivation of slack in the system, a design optimization is performed to generate the key dimensions of the tensioning system that minimizes slack without causing over-constraint. An experimental setup is designed and fabricated to validate the slack predictions in the cable transmission system for a multi-link end-effector, without and with the proposed tensioner. The experimental measurements demonstrate the efficacy of the proposed solution.

1. Introduction and problem motivation

Cable transmissions are commonly used to transmit forces and motion from one location to another in a wide range of mechanical, robotic, and mechatronic applications. Given their small cross-sectional diameter and resulting bending flexibility, cables can be routed through circuitous paths without taking too much space. Common applications include hand-held laparoscopic instruments [1–3], minimally invasive surgery robots [4–11], dexterous manipulators for remote access [12–15], anthropomorphic robotic hands or fingers [16–18], robotic graspers [19], robotic exoskeletons [20], cable driven parallel robots [21,22], consumer products such as 3D printers [23], and aircraft controls [24,25], to name a few.

The input-output relation of any transmission system is critical to its functionality and performance. For a given input motion, a predictable and reliable output motion under various loading conditions is desirable. Compliance in the various transmission members and the reference ground can lead to finite transmission stiffness, which means that for a fixed input, the output can deflect under an output load. Furthermore, gaps in various joints or lack of positive engagement can lead to backlash in the transmission. This implies that for a fixed input, the output can freely move over a finite range of motion (i.e. dead-band).

In the case of a linkage transmission, the relation between the input and output is fully defined by the geometry of the links with the assumption that the links are rigid and the joints have no gaps. In other words, linkage transmission systems have a *kinematic* input-output relation that is ideally independent of the loading conditions. Links can generally be designed to be sufficiently stiff. Backlash, which is the consequnece of necessary gaps in joints and interfaces to avoid jamming, can be greatly optimized to a sufficiently low value. Similarly, gear

* Corresponding author.
E-mail address: awtar@umich.edu (S. Awtar).

https://doi.org/10.1016/j.precisioneng.2021.04.010
Received 31 October 2020; Accepted 18 April 2021
Available online 10 May 2021

transmissions provide a kinematic relation with high transmission stiffness and low backlash. Consequently, these linkage and gear transmissions can be used to effectively transmit force, motion and energy from the input to the output. But the key challenge in these types of transmissions is that they are hard to fit in tight spaces. For example, the use of linkage or gear transmissions in laparoscopic intruments for minimally invasive surgery can be quite challenging given the tight and complex geometry that the transmission has to be routed through [10,19,26–30]. Such transmissions are not conducive for remote access, dexterous manipulation within tight spaces, and circuitious transmission paths.

In such instances, cable transmissions prove to be a compact, simple, and effective solution as indicated by the wide range of applications listed above. Cables may include wires, ropes, filaments, tendons, etc. Cable transmission systems typically rely on the tension that can be generated in and transmitted via a cable. Once again, using the example of articulating instruments for minimally invasive surgery, cable transmission systems are favorable over linkage or gear transmissions due to their ability to transmit sufficient forces and motion over long distances and be routed through narrow and complicated paths [1–11].

Some downsides of cable transmissions include relatively lower load tranmission capability, greater wear, and lower life, but these can be adequately addressed via careful choice of materials, dimensions, fabrication and assembly. However, the input-ouput relation for a cable transmission remains a matter of concern. If one assumes that: 1. the cables are inextensible (i.e. infinitely stiff in its axial direction while remaining compliant in bending), 2. tension in cables remains positive (i.e. there is no slack), and 3. the cables do not slip, then the input-output relation will be kinematic. But these idealized assumptions are hard to meet and entail signficant performance tradeoffs as noted further below.

Consider one of the simplest examples of a cable transmission shown in Fig. 1a. A single driving pulley at the input is connected to a remote multi-link end-effector at the output by two cables for bidirectional actuation (i.e. clockwise as well as counter clockwise). Depending on the actual construction, these two cables could be two distinct cables or a single cable that is wrapped around the driving pulley. If the application is such that the driving pulley has to turn only over a partial rotation, then the cable may be locked to the driving pulley via a ferrule or crimp to avoid slippage.

As the driving pulley rotates counter clockwise (Fig. 1b), it pulls in a certain amount of cable on the left side and releases the same amount on the right side. Load transmission implies that tension increases in the left side cable and drops in the right side cable. Tension in the right side cable can simply drop to a smaller value if the cable transmission was pre-tensioned, or could drop to zero. As a result of this differential tension on the two sides and finite axial stiffness of the cable, the elastic stretch on the left is greater than that on the right, which can lead to slack on the right side. If the cable were to be infinitely stiff in the axial direction or the transmitted load were zero (both of which are impractical assumptions) this *elastic* component of slack would no longer exist. However, for a multi-link end-effector output, there is also a *kinematic* component of slack that is independent of the cable stiffness or transmitted load. As will be shown analytically in this paper, the kinematics of a multi-link end-effector is such that when it articulates to the left (Fig. 1b), the amount of cable released at the output by the end-effector on the left side (Δ_1) is greater than the amount of amount of cable pulled in on the right side (Δ_2). Thus, even though the driving pulley pulls in a certain length of cable (Δ_1) on the left side and passes it on to the right side, the multi-link end-effector only accepts a smaller length of cable on the right side ($\Delta_2 < \Delta_1$). This leads to a *kinematic* slack component on the right side of the transmission. If the output were to be a pulley instead of a multi-link articulating end-effector, the length of cable pulled in by the driving pulley on the left side would be equal to the length of cable reeled in by output pulley on right side, and consequently there would be no kinematic slack.

But multi-link articulating end-effectors are practically necessary in many applications including laparoscopic and robotic instruments for minimally invasive surgery [1,2,4,5,8], dexterous manipulators [12–14], anthropomorphic hands and fingers [16–18], robotic graspers [19], etc. to provide a greater range of articulation in tight spaces. As a

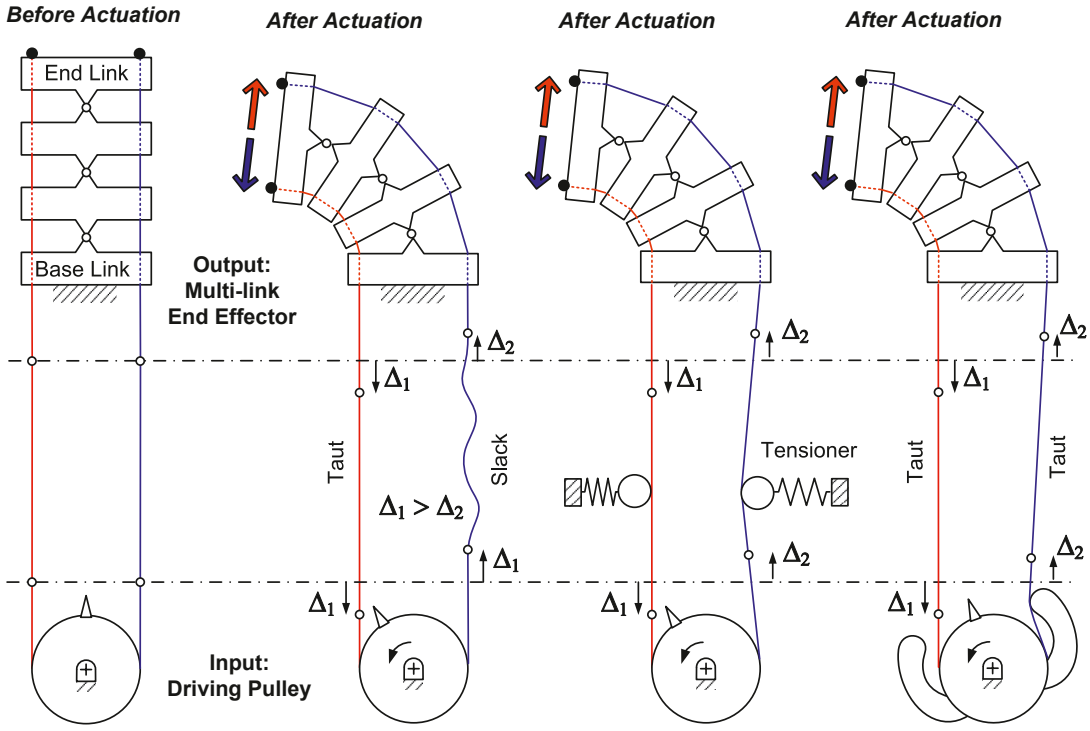

Fig. 1. (a) Cable transmission for remote multi-link end-effector, (b) slack generation on the non-driving side, (c) traditional spring tensioner, and (d) proposed kinematic tensioner.

result, one would expect elastic as well as kinematic components of cable slack in any of these applications – the former due to finite stiffness of the cable and other transmission members, and the latter due to the geometry of a multi-link end-effector.

Cable slack is detrimental to the input-output relation of a cable transmission system. Referring to Fig. 1b, when the input driving pulley is rotated counter clockwise and the end-effector articulates the left to some orientation short of its hard-stops, the transmission stiffness can be assessed by holding the input fixed and applying a load at the output to see if the output moves. An output load applied at the end-effector against the direction of articulation (red block arrow in Fig. 1b) is supported by the left side cable because it is taut. Transmission stiffness in this direction is dependent on the axial stiffness of the cable. On the other hand, when an output load is applied in the direction of articulation (blue block arrow in Fig. 1b), the right side cable, which has slack, is unable to support this load resulting in a low transmission stiffness. In fact, the end-effector can freely move under this load until the right side cable slack is picked up, and then the transmission stiffness is recovered. But in doing so, slack gets generated in left side cable and transmission stiffness in direction of articulation is compromised.

Thus, there exists a backlash at the end-effector wherein for a fixed input, the output can move freely over a range of motion (i.e. dead-band). This leads to a lack of predictability and precision in motion transmission and compromises transmission stiffness and load transmission capability. In case of an articulating instrument for minimally invasive surgery, this limits the ability to position and orient the end-effector precisely, the ability to effectively transmit forces via the end-effectors to the surrounding tissues, and the tactile feedback to the user operating the instrument.

The problem of slack in cable transmissions has been widely recognized [8–11,13,15–17,24], along with the need to maintain positive tension at all times. Similarly, the existence and challenges associated with the backlash in cable transmissions has received considerable attention [10,11,15]. For an articulating multi-link end-effector referred to as a continuous backbone [13], it is shown that the slack generation is minimized when the articulation cable is placed radially farthest from the central axis of the end-effector. But minimizing the generation of slack in this manner would require an end-effector with a larger diameter or more number of links, both of which are undesirable for remote manipulation in tight spaces. Another clever concept to minimize the generation of kinematic slack in the cable transmission of a multi-link articulating end-effector is to employ a unique geometry of the individual links [8]. A non-attached, rolling engagement between two consecutive links is employed to provide a remote center of rotation for each link such that the cable length released on one side is equal to the cable length pulled in on the other side. This concept is difficult to implement in practice because the links are not physically held or pinned together. Also, this arrangement only helps mitigate the kinematic component of slack and does not impact the elastic component.

Other than geometric optimization of the end-effector to minimize slack generation, several ways to absorb slack have been reported in the previous literature but each solution has significant drawbacks or limitations. The most common practice to avoid slack is to pre-tension the cables [9,11,15]. Higher the pre-tension, greater the system's ability to absorb any cable length differential and avoid cable tension becoming zero. While this works for both elastic as well as kinematic components of slack, a high pre-tension leads to greater friction and wear in the system, lowers the transmission efficiency, and increases chances of failure. Greater frictional resistance is particularly problematic in manually driven manipulators because it impacts user ergonomics and tactile feedback.

More sophisticated springs based designs for picking slack and maintaining tension in cable transmissions have been presented in the context of aircraft controls e.g. operating engine throttles, controlling surfaces such as ailerons, elevators, and rudders, and propeller feathering mechanisms [24,25]. These designs employ a combination of springs and clutches to ensure that the springs act to pick up slack on the non-driving or loose side of the cable transmission without impacting the driving side which remains taut. While promising, these designs are difficult to implement in applications such as surgical instruments and robots where space is tight.

Another commonly employed solution is to include spring-loaded tensioners along the transmission [31]. As shown in Fig. 1c, the tensioner picks up any slack that develops on either side of the transmission as a result of the driving pulley actuation. However, greater the expected slack in the system, greater the pre-compression in the springs. This means that in the nominal unactuated condition, the spring-tensioners apply the maximum lateral force on the cable leading to higher cable tension, which has disadvantages similar to the high pre-tension listed above. Also, there remains a tradeoff with transmission stiffness. When the input driving pulley is rotated counter clockwise and the end-effector articulates the left, an output load applied at the end-effector against the direction of articulation (red block arrow in Fig. 1c) is supported by the tension in the left side cable. But an output load applied at the end-effector in the direction of articulation (blue block arrow in Fig. 1c) is supported by the stiffness of the tension spring on the right side cable. If this spring stiffness is too low, then the transmission stiffness in this direction remains sub-optimal. If the spring stiffness is too high, then the nominal tension in the cables goes up, resulting in greater friction, wear and chances of failure and lower transmission efficiency.

Another possible solution to address some of the symptoms of slack, namely backlash and stiffness at the end-effector, is to add spring elements at the end-effector itself [4,5,12,13] but this leads to several tradeoffs. While this eliminates the free movement of the end-effector and makes the end-effector resistant to output loads, the associated stiffness is now dictated by the end-effector spring and not the cables. A high spring stiffness improves the output load resisting capability of the end-effector but the same time increases the actuation effort at the driving pulley and reduces tactile feedback. Also, this solution does not address the dead-band in the input-output relation of the cable transmission.

Yet another solution is to make sure of additional actuators to make sure that tension in each cable is independently controlled [11,15,18,27]. For example, in the case of the cable transmission in Fig. 1a, instead of using a single driving pulley to control both the right side and left side cables (i.e. bidirectional actuation), two driving pulleys may be employed, one each for the right and left side cables. This allows for controlling tension in both the cables and ensuring that there is never any slack in any of the cables. Although this adds cost and design complexity, this can serve a solution for robotic manipulators where there is room for multiple actuators (e.g. motors) on the input side. However, this is impractical for compact as well as manually driven instruments and manipulators where there is only one input actuator available for one output motion.

In this paper, we present a simple solution that can effectively mitigate slack on the non-driving side of a cable transmission between a driving pulley and a multi-link end-effector, without additional cost or complexity. The proposed design uses a modified driving pulley (with tensioner extensions) to alter the transmission path, which provides a kinematic or geometric solution in contrast to the various spring based solutions listed above that have several limitations. This kinematic tensioner can be seen in Fig. 1d, where the driving pulley has rigid extensions that act from the outside of the cable. As this modified driving pulley rotates to actuate the end-effector, the right side tensioner extension moves into the slack side of the transmission and forces the cable between the pulley and end-effector to take a longer path, thus absorbing any excess cable length, i.e. slack, in the process. At the same time the left side tensioner lifts off the left side cable and therefore doesn't impact the already taut cable. The reverse happens when the driving pulley is rotated clockwise. Even though this solution is kinematic, it is effective in mitigating the kinematic as well as elastic

components of slack in a cable transmission with finite input rotation.

The increase in the cable path length produced by the tensioner should ideally be equal to the slack generated in the cable if there were no tensioner. Thus, designing the tensioner involves calculating the optimal values of geometric parameters such as the tensioner extension radius and its distance from the pulley center for given geometric parameters of the rest of the transmission system (e.g. driving pulley diameter and end-effector dimensions). The first step in that direction is to analytically quantify slack in the system in terms of geometric parameters of the input and output, which is the focus of Section 2.

The representative multi-link end-effector considered in this paper has two orthogonal planes of articulation *P1* and *P2*, as shown in Fig. 2. Three alternating links are responsible for motion in each plane of actuation with a total of six links arranged alternately. This allows independent articulation control of the end-effector in the two orthogonal planes. The motion along each plane of motion is controlled by a respective driving pulley via a respective cable transmission that goes through all intermediate links of the end-effector and is attached to the final link.

The remainder of the paper is organized as follows: Section 2 presents the closed form analytical formulation of kinematic slack in the cable transmission of a multi-link end-effector. Section 3 addresses the analysis and design of the proposed tensioning system. Section 4 presents the experimental setup for the purpose of validating the model for slack and the effectiveness of the tensioning system. Section 5 provides concluding remarks and future work.

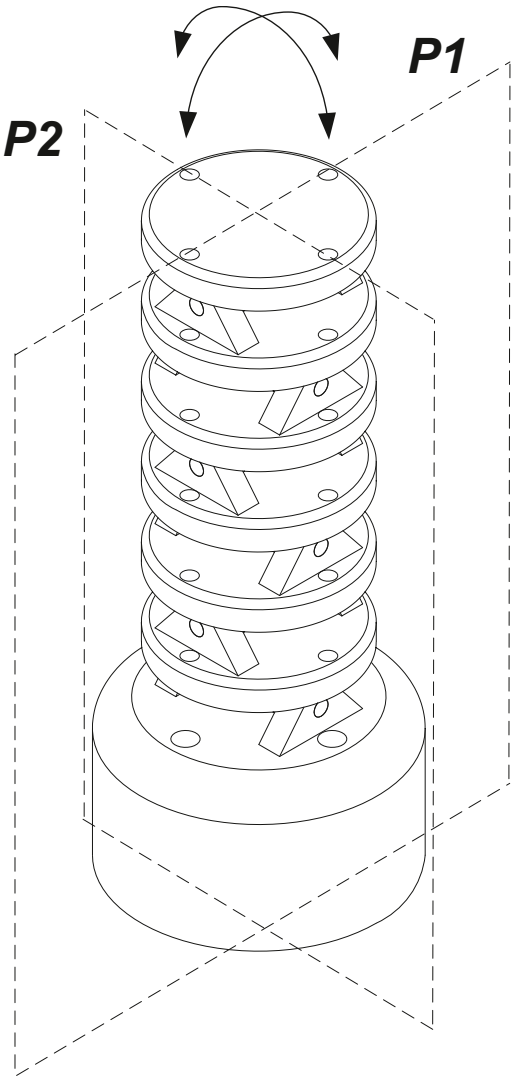

Fig. 2. Multi-link end-effector.

2. Slack formulation via kinematic modeling

This section presents an analytical formulation of slack in the cable transmission of the system. Once the slack is determined for a single link pair, the slack in the entire system can be determined as a function of the angles made by the individual links of the end-effector. Ultimately, a closed form expression for slack is obtained that relates it to the input pulley (i.e. driving pulley) angle. For the purpose of this analysis, the actuation of one link pair is considered (Fig. 3). Fig. 3a shows the initial condition of a single link pair and Fig. 3b shows the link position as a result of counter clockwise actuation. Link *CD* can rotate about pivot *P* and is actuated via cables *KL* and *MN* wrapped around an input pulley (not shown). The angle made by link *CD* relative to the base link *AB* is θ. The moment arm (*PR*) of the rotation of link *CD* is of length *g*. The initial length of cables *KL* and *MN* is *2g* located at radial distance *a* from the central axis. Upon actuation to angle θ, the lengths of cables *KL* and *MN* become $2g_1$ and $2g_2$ respectively. Slack is generated in the transmission because the change in length of *KL* is not equal to the change in length of *MN*. The difference between the length of cable passed on by *KL* and length of cable accepted by *MN* is defined as the kinematic slack in the transmission. This difference causes the cable on the *MN* side of the transmission to lose tension. Similar reasoning can be used to explain the onset of slack on the *KL* side of the transmission for clockwise actuation.

2.1. Ideal Model (IM)

The change in length of cable *KL* is given by,

$$\Delta_1 = 2(g - g_1) \tag{1}$$

The change in length of cable *MN* is given by,

$$\Delta_2 = -2(g - g_2) \tag{2}$$

From equations (1) and (2) the slack generated from a single link pair is given by,

$$Slack = (\Delta_1 - \Delta_2) = 4g - 2(g_1 + g_2) \tag{3}$$

In order to quantify the slack in terms of the geometric parameters of the links, we see from Fig. 3b that,

$$RQ = \frac{1}{2}(KL + MN) = (g_1 + g_2) = 2g\cos\left(\frac{\theta}{2}\right) \tag{4}$$

Substituting (4) in (3), an expression for slack per link pair is obtained as a function of the link angle θ and parameter *g*,

$$Slack = 4g\left[1 - \cos\left(\frac{\theta}{2}\right)\right] \tag{5}$$

Expression (5) gives the slack generated when a single link rotates by an angle θ with respect to its previous link. It may be noted that the above analysis is idealized in the sense that cables are represented as lines and the holes on the links through which they pass are considered as points. This model is referred to as the *Ideal Model* (IM). In reality of course, cables and holes will have finite diameters and will be taken into account in subsequent analyses.

Relation (5) can now be extended to the case where *n* links are stacked one over the other as shown in Fig. 4, such that the i^{th} *link pair* $(L_i - L_{i+1})$ subtends an angle θ_i; the total slack in the transmission would thus be the sum of slack contributions from each link pair and given by,

$$Slack_{total} = 4g\left\{(n-1) - \sum_{i=1}^{n-1}\cos\left(\frac{\theta_i}{2}\right)\right\} \tag{6}$$

Expression shows that upon actuation, the total kinematic slack in the system depends on all individual link pair angles and is zero only

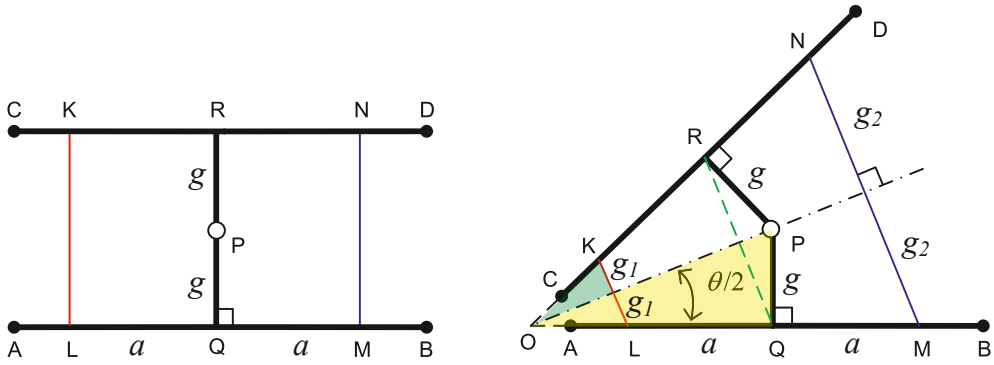

Fig. 3. Single link pair (a) before actuation (b) after actuation.

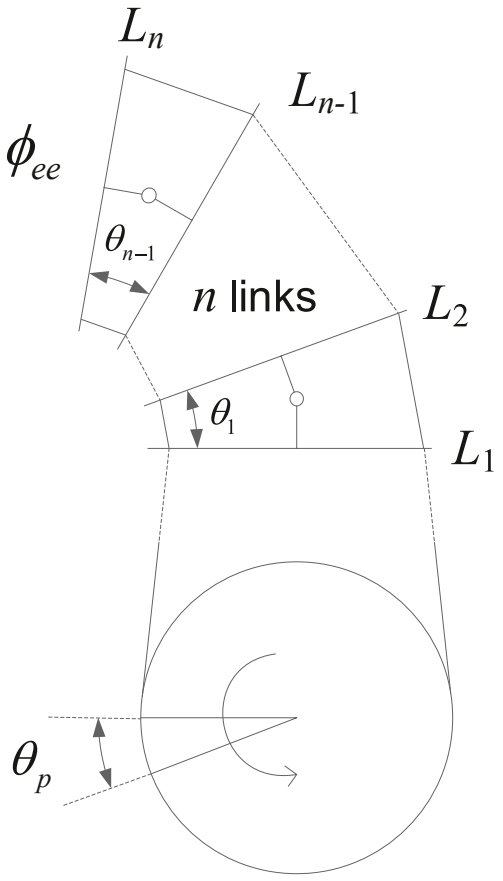

Fig. 4. Actuation of n-link end-effector.

when the axial length g of the link goes to zero. For practical reasons, it is difficult to make g zero in a physical embodiment of a multi-link end-effector. Ref [8] tries to accomplish this via a non-attached, rolling engagement between two consecutive links to project a remote center of rotation that makes g virtually zero for each link, but this concept is difficult to implement in practice.

It is worthwhile to note that even though an *n-link* end-effector has *(n-1)* degrees of freedom in a single plane of actuation with the base link (L_1) grounded, a single pulley controls the end-effector through the cable transmission such that the cables pass through all intermediate links and are only connected to the ultimate end-effector link (L_n), making the system under-actuated. Thus, even though the overall output angle of the end-effector (ϕ_{ee}) is determined for a given input angle θ_p, the orientation of the intermediate links and thus the slack in the system is non-unique.

However, a range of slack variation with respect to pulley angle (θ_p) can still be determined. To characterize this range, one can extremize the slack function to find its minimum and maximum bounds. It is observed from (6) that for a given input or output angle, slack is maximum when the summation of cosine terms is minimum and vice versa. This extremization problem, subject to various constraints, can be stated as follows:

$$\text{Extremize } f(\theta_i) = \sum_{i=1}^{n-1} \cos(\theta_i / 2) \tag{7}$$

The equality constraint for this problem is that the sum of all the link pair angles amounts to the total output angle ϕ_{ee} and the inequality constraints are the physical angle limits $\theta_{\max}$ imposed on each individual link pair angle by the geometry of the links. Non-negative constraints are imposed on all individual link pair angles. Referring to Fig. 3,

$$\theta_{\max} = 2\tan^{-1}\left(\frac{g}{a}\right) \tag{8}$$

It can be seen that ϕ_{ee} can physically take on a maximum value of $(n-1)\theta_{\max}$.

For the sake of illustration, we look at the case of a three-link end-effector. To incorporate the equality and inequality constraints in the extremization problem, the following Lagrangian is constructed whereλ and μ_i are Lagrange multipliers:

$$\mathscr{L}(\theta_i,\mu_i,\lambda) = \sum_{i=1}^{2} \cos\left(\frac{\theta_i}{2}\right) + \lambda\left(\phi_{ee} - \sum_{i=1}^{2}\theta_i\right) + \sum_{i=1}^{2}\mu_i(\theta_{\max} - \theta_i) + \mu_3\theta_1 + \mu_4\theta_2 \tag{9}$$

(a) When both angles θ_1 and θ_2 are within their ranges of 0 and $\theta_{\max}$, the inequality constraints are not active (i.e.$\mu_1 = \mu_2 = \mu_3 = \mu_4 = 0$) and the stationary points of the Lagrangian are given by:

$$\frac{\partial \mathscr{L}}{\partial \theta_1} = -\frac{1}{2}\sin\frac{\theta_1}{2} - \lambda = 0 \tag{10}$$

$$\frac{\partial \mathscr{L}}{\partial \theta_2} = -\frac{1}{2}\sin\frac{\theta_2}{2} - \lambda = 0 \tag{11}$$

$$\frac{\partial \mathscr{L}}{\partial \lambda} = (\phi_{ee} - \theta_1 - \theta_2) = 0 \tag{12}$$

The extremization leads to the solution:

$$\theta_1 = \theta_2 = \frac{\phi_{ee}}{2}$$

(b) When one of the inequality constraints is active (i.e. $\theta_1 = 0$ and therefore $\mu_1 \neq 0$) and the others are inactive (i.e. $\mu_2 = \mu_3 = \mu_4 = 0$ and therefore θ_2 is within its range of 0 and $\theta_{\max}$), the extremization of Lagrangian leads to the solution:

$$\theta_1 = 0 \text{ and } \theta_2 = \phi_{ee}$$

An equivalent extremization is the complement of this, i.e.

$\theta_1 = \phi_{ee}$ and $\theta_2 = 0$

(c) When one of the other inequality constraints is active (i.e. $\theta_1 = \theta_{max}$ and therefore $\mu_3 \neq 0$) and the others are inactive (i.e. $\mu_1 = \mu_2 = \mu_4 = 0$ and therefore θ_2 is within its range of 0 and θ_{max}), the extremization of Lagrangian leads to the solution:

$\theta_1 = \theta_{max}$ and $\theta_2 = \phi_{ee} - \theta_{max}$

An equivalent extremization is the complement of this, i.e.

$\theta_1 = \phi_{ee} - \theta_{max}$ and $\theta_2 = \theta_{max}$

Solution (a) provides the minimum slack condition, while solutions (b) and (c) provide the maximum slack condition. Solution (a) shows that for a desired output angle ϕ_{ee}, minimum slack is obtained if this desired output is achieved by orienting each link pair by equal angles. Solution (b) applies when $\phi_{ee} \leq \theta_{max}$ and corresponds to one link pair remaining at zero angle and the entire output angle appearing at the other link pair when $\phi_{ee} \leq \theta_{max}$. Solution (c) applies when $\theta_{max} < \phi_{ee} \leq 2\theta_{max}$ and corresponds to one link pair having reached its physical limit, while the other link pair assuming the remaining output angle.

It can be shown that, in general, for an n-link end-effector, the minimum kinematic slack occurs when:

$$\theta_i = \frac{\phi_{ee}}{(n-1)};\ 1 \leq i \leq (n-1) \tag{13}$$

For a given constant sum of angles, the summation of their cosines is greatest (corresponding to minimum slack), when each of the individual angles are equal to each other. Henceforth, this condition will be referred to as *equal angle actuation*. As for the minimum of the cosine summation (corresponding to maximum slack), that depends on the constraint imposed on the maximum value that each individual angle can take. Physically, if the desired output angle ϕ_{ee} is smaller than the angle limit θ_{max} for a single link pair, the minimum cosine sum will occur when any one of the link pair angles takes on the value ϕ_{ee}while all other angles remain zero. If, however, the output angle ϕ_{ee} is greater than θ_{max} but less than $2\theta_{max}$, the minimum summation, given the constraints, would occur when any one of the link pair angles takes on the value θ_{max} and any one of the other angles takes on $(\phi_{ee} - \theta_{max})$ while all others remain zero. This trend continues for subsequent value ranges of ϕ_{ee}. Henceforth, this condition will be referred to as *step-wise actuation* because this physically corresponds to a situation where, in order for maximum slack to exist throughout the actuation of the end-effector, individual links must actuate consecutively, one at a time, only after the previous link pair has reached its physical limit. This may be stated mathematically as follows: For an output angle $m\theta_{max} \leq \phi_{ee} \leq (m+1)\theta_{max}$ where $m = 0 \ldots (n-2)$, slack is maximum when

$$\theta_i = \left\{ \begin{array}{ll} \theta_{max} & \text{for } m \text{ of the angles} \\ \phi_{ee} - m\theta_{max} & \text{for 1 of the angles} \\ 0 & \text{for remaining } (n-m-2) \text{ angles} \end{array} \right\} \tag{14}$$

Equal angle actuation

Now that it has been established that an equal angle actuation of the end-effector links yields minimum slack in the system, an exact formulation of slack with respect to the input pulley angle can obtained. This formulation establishes the lower-bound of possible slack in the system for a given pulley input. To obtain a relationship between the slack and the input pulley angle θ_p, it is identified that during actuation, the cable length on the driving side of the transmission is conserved. This means that the cable length pulled in by a driving pulley of radius r_p that has rotated by angle θ_p equals the total change in length of the cable on the driving side. This analysis assumes that there is no slip between the cable and pulley, the cables are inextensible, and that there is total decoupling between the orthogonal planes of actuation of the end-effector. Expression (13) is first substituted in to obtain total slack in terms of the output angle for the case of equal angle (EA) actuation of the end-effector links.

$$Slack_{EA} = 4g\left(n-1\right)\left[1 - \cos\left(\frac{\phi_{ee}}{2(n-1)}\right)\right]; \tag{15}$$

For a single link pair, the link geometry leads to:

$$\Delta_1 = 2g\left[1 - \cos\left(\frac{\phi_{ee}}{2(n-1)}\right)\right] + 2a\sin\left[\frac{\phi_{ee}}{2(n-1)}\right] \tag{16}$$

Cable length conservation is given by,

$$r_p\theta_p = (n-1)\Delta_1; \tag{17}$$

Substituting (16) in (17),

$$\frac{\phi_{ee}}{2(n-1)} = \sin^{-1}\left(\left(\frac{\theta_p}{(n-1)} - \frac{2g}{r_p}\right).\frac{1}{\left(A^2+B^2\right)^{1/2}}\right) - \tan^{-1}\left(\frac{A}{B}\right) \tag{18}$$

where,

$$A = \frac{-2g}{r_p} \text{ and } B = \frac{2a}{r_p} \tag{19}$$

Relation (18) computes the output angle ϕ_{ee} for a given pulley input angle θ_p assuming equal angle actuation of the links. This expression can now be substituted in the total slack equation (15) to given the total slack in the system in terms of the input pulley angle during equal angle (*EA*) actuation.

$$Slack_{EA} = 4g\left(n-1\right)\left[1 - \cos\left(\sin^{-1}\left(\left(\frac{r_p\theta_p}{2(n-1)} - g\right).\frac{1}{\left(g^2+a^2\right)^{1/2}}\right) - \tan^{-1}\left(\frac{-g}{a}\right)\right)\right] \tag{20}$$

Thus slack is obtained as a function of geometric quantities g, a, n and r_p, and the variable pulley angle θ_p. It is interesting to note that if the values of g, a and r_p were scaled by a common factor while keeping the number of links n the same, the slack in the system would get scaled by exactly the same factor, implying that using an end-effector and pulley that are twice as big would result in twice the slack in the transmission for equal angle actuation. Such a linear scaling relation between the geometric dimensions and slack greatly helps in experimentation as measurements done on a large scale system can help in drawing conclusions about an equivalent but scaled down system.

Under-actuation of a multi-link end-effector by a single pulley is well-recognized in the literature and various methods to achieve equal angle actuation have been implemented. The most common among these is to employ spring action in the end-effector that averages out the total output angle among all the link pairs [4,5,12,13]. Another method involves actuating the various links individually to minimize under-actuation [1,4,12].

Step-wise actuation

Previously, the extremization of the slack function revealed that it was maximum when the links of the end-effector were actuated step-

wise for any given end-effector angle. For this type of actuation, a single link pair actuates at a time. The other link pairs remain un-actuated till the actuating pair reaches its physical angle limit θ_{max}. It is only when the previous link pair reaches this limit that the next link pair begins actuation, and so on. Considering the actuation of the first link pair (L_1 - L_2), the total slack in the system is simply the slack contribution due to actuation of the first link pair until it reaches θ_{max}. The expression for system slack for the duration of actuation of the first link pair is given by relation (20), by substituting $n = 2$.

$$Slack_{L_1-L_2} = 4g\left[1-\cos\left(\sin^{-1}\left(\left(\frac{r_p\theta_p}{2}-g\right).\frac{1}{(g^2+a^2)^{1/2}}\right)-\tan^{-1}\left(\frac{-g}{a}\right)\right)\right] \tag{21}$$

Once the first link pair reaches its angle limit, the second link pair begins to actuate. The system slack in this case is the slack due to the actuation of the second link pair in addition to the already existing slack from the actuation of the first link pair. Knowing that the physical angle limit for any given link pair is θ_{max}, the portion of slack contributed by the fully actuated first link pair is given by equation (5),

$$Slack = 4g\left[1-\cos\left(\frac{\theta_{max}}{2}\right)\right] \tag{22}$$

Equations (21) and (22) are combined to yield a general total slack expression in the system for a given pulley angle θ_p due to step-wise (SW) actuation.

$$Slack_{SW} = 4\ g\ m\left[1-\cos\left(\frac{\theta_{max}}{2}\right)\right]+4g\left[1-\cos\left(\sin^{-1}\left(\left(\frac{r_p(\theta_p-m\ \theta_{p\_max})}{2}-g\right).\frac{1}{(g^2+a^2)^{1/2}}\right)-\tan^{-1}\left(\frac{-g}{a}\right)\right)\right] \tag{23}$$

$$\theta_{p\_max} = \left[\frac{2g}{r_p}\left(1-\cos\left(\frac{\theta_{max}}{2}\right)\right)+\frac{2a}{r_p}\sin\left(\frac{\theta_{max}}{2}\right)\right] \tag{24}$$

In expression (23), θ_{p_max} corresponds to the input pulley angle for which a single link pair reaches its physical angle limit and can be determined from equation (24) which was obtained from equation (17). 'm' equals the number of link pairs that have reached their physical angle limit during the course of end-effector actuation.

Relations (20) and (23) form the lower and upper bounds, respectively, for possible slack in the system during actuation, for a given pulley angle θ_p. The indeterminism of exact slack in the system lies in the fact that the system consists of $(n-1)$degrees of freedom per plane of actuation but only a single actuator per plane. If each link were controlled by individual pulleys or kinematically constrained with each other while using a single pulley [1,4], the forward kinematics and therefore slack variation with pulley angle would become fully deterministic.

As mentioned before, the above analysis does not factor the possibility of lateral play between the cables and the holes in the end-effector links through which they pass. The subsequent analysis will consider this effect and augment the slack expressions, revealing a more realistic range of slack variation with driving pulley angle.

2.2. Realistic model (RM)

Next, we modify the Ideal Model for slack in order to make it more reflective of real effects such as finite cable diameter and slightly larger finite diameter of holes in the end-effector links through which these cables pass. Consider a single link pair after counter clockwise driving pulley rotation, which results in the orientation shown in Fig. 5. The real effects cause the cables to shift their axes away from their respective hole axes towards the hole edges. This offset from the hole axes can vary depending on the degree of actuation, but Fig. 5 shows the extreme case when the cable makes contact with the hole edge. Let d_c and d_h be the diameters of the cable and hole respectively. It can be observed that the cable axes are no longer symmetrically placed on either side of the pivot P after actuation.

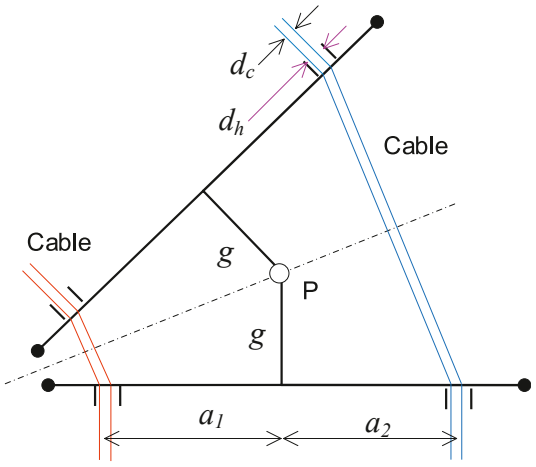

Fig. 5. Single link pair with real effects.

$$a_1 = a + h \quad \text{and} \quad a_2 = a - h \tag{25}$$

where, $h = \frac{d_h - d_c}{2}$

Following a method similar to the one used to derive slack in relation (5), a modified expression for slack is obtained:

$$Slack^{RM} = 4g\left[1-\cos\left(\frac{\theta}{2}\right)\right]+4h\sin\left(\frac{\theta}{2}\right) \tag{26}$$

As can be seen from relation (26), the term $4h\sin\left(\frac{\theta}{2}\right)$ causes the predicted slack in this model to be greater than in the Ideal Model discussed previously, for the same link angle and a single link pair. Henceforth, this model will be referred to as the *Realistic Model* (RM). It may be noted that this model addresses an extreme condition of the cable transmission during actuation. In reality, the cable transmission may see a combination of equal angle and step-wise actuation; some link pairs may see the cable axes displaced from the hole axes to some degree and others may not. The sole endeavor of this type of modeling is to establish realistic ranges within which the actual slack may vary. Relation (26) may now be simplified to yield a single trigonometric function to give,

$$Slack^{RM} = 4g\left[1+\left(1+\left(\frac{h}{g}\right)^2\right)^{1/2}\sin\left(\frac{\theta}{2}+\psi\right)\right] \tag{27}$$

$$\text{where } \psi = \tan^{-1}\left(\frac{-g}{h}\right) \tag{28}$$

One way to verify relation (27) is to observe that as $h \to 0$,

$Slack \rightarrow 4g\left(1-\cos\left(\frac{\theta}{2}\right)\right)$ which was initially derived in the Ideal Model. This analysis also clearly shows that minimizing play between the cable and hole helps reduce slack in the overall system. However, the tradeoff is increased friction, wear, and chances of cable failure.

Generalizing the slack expression (27) for n-links,

$$Slack_{Total}^{RM} = 4g\left[(n-1)+\left(1+\left(\frac{h}{g}\right)^2\right)^{1/2}\sum_{i=1}^{n-1}\sin\left(\frac{\theta_i}{2}+\psi\right)\right] \tag{29}$$

Using an analysis similar to that used for the Ideal Model, slack expressions for equal angle and step-wise actuation can be obtained for the Realistic Model (RM) and are given below.

Equal angle actuation

$$Slack_{EA}^{RM} = 4g\left(n-1\right)\left[1+\sqrt{1+\left(\frac{h}{g}\right)^2}\sin\left(\sin^{-1}\left(\left(\frac{r_p\theta_p}{2(n-1)}-g\right)\cdot\frac{1}{\sqrt{(g^2+a_1{}^2)}}\right)-\tan^{-1}\left(\frac{-g}{a_1}\right)+\psi\right)\right] \tag{30}$$

Step-wise actuation

$$Slack_{SW}^{RM} = 4gm\left[1+\sqrt{1+\left(\frac{h}{g}\right)^2}\sin\left(\frac{\theta_{\max}}{2}+\psi\right)\right]$$
$$+4g\left[1+\sqrt{1+\left(\frac{h}{g}\right)^2}\times\sin\left(\sin^{-1}\left(\left(\frac{r_p(\theta_p-m\theta_{p\_\max})}{2}-g\right)\cdot\frac{1}{\sqrt{g^2+a_1{}^2}}\right)\right.$$
$$\left.-\tan^{-1}\left(\frac{-g}{a_1}\right)+\psi\right)\Bigg] \tag{31}$$

where,

$$\theta_{p\_\max} = (n-1)\left[\frac{2g}{r_p}\left(1-\cos\left(\frac{\theta_{\max}}{2}\right)\right)+\frac{2a_1}{r_p}\sin\left(\frac{\theta_{\max}}{2}\right)\right]$$

The system under consideration has the following geometric parameters in inches:

$a = 0.2952$, $g = 0.0897$, $r_p = 1$, $n = 4$; $d_h = 0.059$, $d_c = 0.038$;

Using these values, plots of the slack variation over input pulley actuation predicted by the Ideal Model (IM) and the Realistic Model (RM) are shown in Fig. 6. For both equal angle as well as step-wise actuation, the Realistic Model predicts a larger variation in slack over input pulley actuation, as discussed previously, due to the extra term in the slack formulation arising from the lateral play between the cables and the holes in the links that they pass through. The maximum predicted slack, occurring when all link pairs have reached their respective physical angle limits, is nearly doubled in the Realistic Model compared to the Ideal Model for a hole diameter that is about 55% larger than the cable diameter. From the plots of slack variation for step-wise actuation in both models, one can see the sharp points at which one link pair reaches its physical angle limit and further pulley rotation causes another link pair to actuate, thus causing slack to further accumulate. The step-wise actuation formulation poses no constraint on the order in which the link pairs get actuated, as long as they are actuated one at a time. The final slack from equal angle and step-wise actuation is of the same magnitude in both the models because at this point, all links have reached their physical angle limit and this is the only configuration that corresponds to the maximum output angle of $\phi_{ee} = (n-1)\theta_{\max}$.

The solid purple line and dashed green line in Fig. 6 provide the range or envelope within which slack in the system could vary depending on the combination of equal angle and step-wise actuation of the end-effector and whether cables have remained co-axial with the holes in some link pairs and have deviated from hole axes in others. This completes the kinematic analysis of the slack generated in the cable transmission of a multi-link end-effector. The next section presents the

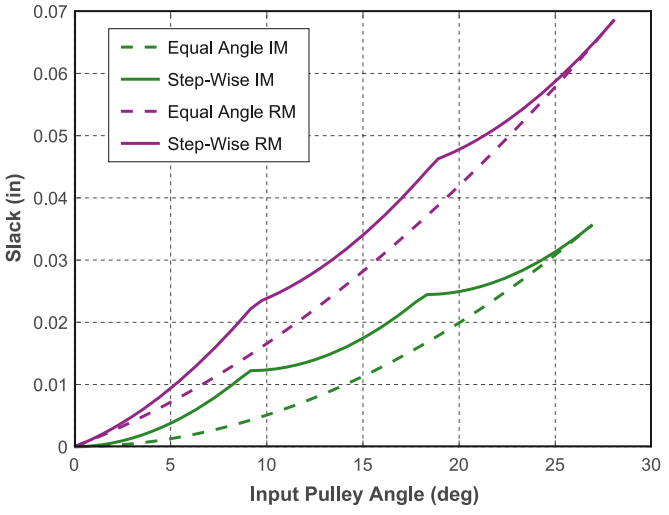

Fig. 6. Range of Slack Variation over Input Pulley Actuation using Ideal Model (IM) and Realistic Model (RM).

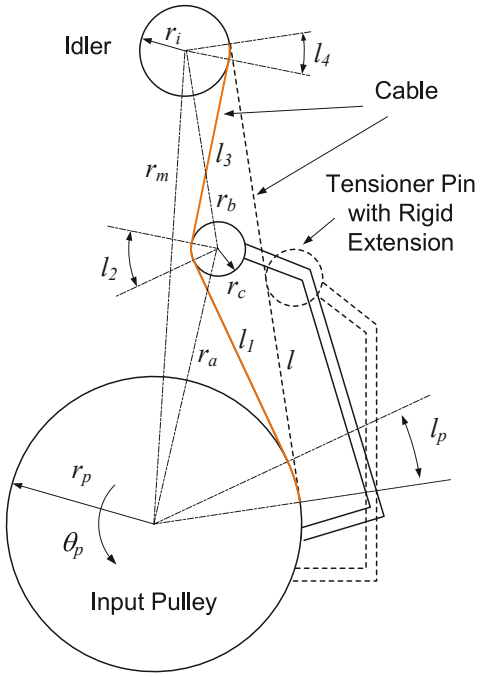

Fig. 7. Tensioner geometry and action.

synthesis of the proposed kinematic tensioner to optimally take up this slack in the transmission system.

3. Tensioner design

This section addresses the design of the proposed kinematic tensioning system to minimize slack in the cable transmission. The concept of the tensioner along with a geometric representation of the same is shown in Figs. 1d and 7, respectively. The tensioner comprises a tensioner pin that is connected to the input pulley by means of a rigid extension and is initially tangential to the cable. A set of idlers isolate the tensioning system from the rest of the cable transmission. The geometric representation in Fig. 7 shows only one side of the transmission, the side that experiences slack during counter clockwise actuation. Due to the presence of the tensioner, the cable between the input pulley and the idler is made to take on a larger length than if there were no tensioner. If this increase in length of the cable path equals the slack generated in the transmission, the tensioner would have absorbed exactly the required length of cable to keep it in tension. The following analysis assumes inextensibility of the cables and that the two orthogonal planes of end-effector actuation are completely decoupled. The tangent length l, between the pulley and idler, is the nominal length of the cable before actuation. With the tensioner in place, the new cable length (showed in orange) upon actuation would be:

$$l_{new} = \left(l_p + l_1 + l_2 + l_3 + l_4\right) \tag{32}$$

Consequently, the slack removed from the system or the 'tensioner action' (l_t) is given by:

$$l_t = l_{new} - l \tag{33}$$

In the previous section, transmission slack was formulated as a function of the pulley angle for equal angle and step-wise actuation. We now formulate the tensioner action (l_t) as a function of the input pulley angle θ_p and pertinent geometric variables of the system such as the input pulley radius (r_p), tensioner pin radius (r_c), idler radius (r_i), center to center distance between the input pulley and tensioner pin (r_a) and the center to center distance between the input pulley and the idler (r_m). Via the geometry of the system, the following relations are determined.

$$l = \left({r_m}^2 - \left({r_p}^2 - {r_i}^2\right)\right)^{1/2} \tag{34}$$

$$l_p = l_p \theta_p \tag{35}$$

$$l_1 = \left(r_a^2 - \left(r_p + r_c\right)^2\right)^{1/2} \tag{36}$$

$$l_2 = r_c\left(\theta_p + C\right) \tag{37}$$

$$l_3 = \left(r_b^2 - \left(r_i + r_c\right)^2\right)^{1/2} \tag{38}$$

$$l_4 = r_i C \tag{39}$$

where,

$$r_b = {r_a}^2 + {r_m}^2 - 2 r_a r_m \sin\left[\theta_p + \sin^{-1}\left(\frac{r_p - r_i}{r_m}\right) + \cos^{-1}\left(\frac{r_p + r_c}{r_a}\right)\right] \tag{40}$$

$$C = \sin^{-1}\left(\frac{r_p - r_i}{r_m}\right) + \sin^{-1}\left(\frac{r_i + r_c}{r_b}\right) - \sin^{-1}\left[\frac{r_a}{r_b}.\cos\left(\theta_p + \sin^{-1}\left(\frac{r_p - r_i}{r_m}\right) + \cos^{-1}\left(\frac{r_p + r_c}{r_a}\right)\right)\right] \tag{41}$$

Substituting (34)–(39) in (33), the tensioner action is obtained with respect to input pulley angle and geometric parameters of the transmission system.

In order to determine the appropriate tensioner geometry (r_c and r_a) to reduce slack in the non-driving side of the cable, the RMS of the error function (e), which is the difference between the tensioner action (l_t) and slack (*Slack*) in the transmission, is considered as the objective function (f) to be minimized.

$$e = l_t - Slack \tag{42}$$

$$\text{Minimize: } f = \left(\frac{1}{k}\sum_{j=1}^{k}\left(e(j)\right)^2\right)^{1/2} \tag{43}$$

While optimizing the tensioner geometry, the slack initially considered in the error function is that yielded by equal-angle actuation predicted by the Ideal Model because this is the minimum slack predicted in the transmission (green dashed line in Fig. 6). If the error is calculated with respect to more aggressive slack estimates such as step-wise actuation in either model or equal angle actuation in the Realistic Model, then the optimized tensioner geometry may result in an over-constraint in the actuation mechanism. The input pulley will actuate the end-effector via the cables, but as the tensioner absorbs slack, it may tend to remove more slack than what is generated in the system, thus potentially jamming the transmission. Thus, for the present exercise, a match is attempted between the tensioner action curve and the equal-angle actuation curve from the Ideal Model. In general, the choice of slack estimate used in (42) depends on the application, the material and compliance of the cable and other components, dimensions and tolerances, and the judgement of the designer. Also, while the present analysis only assumes kinematic slack, one may also include elastic slack in the optimization performed to determine the dimensions of the tensioner.

In expression (43), 'k' is the number of data points over the range of actuation over which the RMS error is computed and minimized. The geometric constraints imposed on the problem must ensure that all physical impossibilities are discounted. A non-negative constraint is applied to the tensioner radius. A minimum constraint is applied to the center to center distance of the tensioner and the input pulley as the tensioner center must lie outside the pulley diameter for a valid physical embodiment of the tensioning system. Finally, two maximum constraints are applied to the tensioner radius, one related to the input pulley and the other related to the idler pulley. These constraints are quantified as follows:

$$r_c \geq 0 \text{ and } r_a \geq r_p \tag{44}$$

$$r_c \leq \left(r_a - r_p\right) \text{ and } r_c \leq \frac{r_m - \left(r_p + r_i\right)}{2} \tag{45}$$

The above optimization model was set up in MS Excel and solved

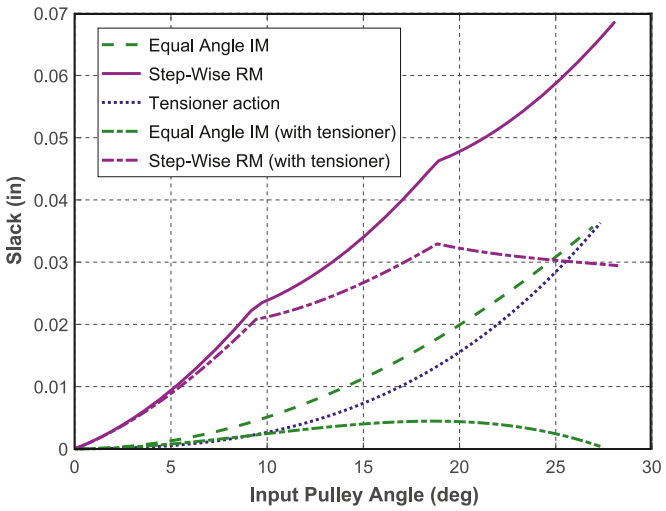

Fig. 8. Range of slack variation region due to tensioner action.

using the Generalized Reduced Gradient (GRG) nonlinear solver. A locally optimal solution was obtained assuming the following values of input pulley radius, idler radius, and the idler location.

Geometry (inches)

$$r_p = 1; r_i = 0.144 \tag{46}$$

Location of idler pulley center w.r.t. input pulley center:$(x_i, y_i) = (0.5, 3)$ (47).

Optimal solution (inches)

$$r_c = 0.09575; r_a = 1.1; f = 0.0029 \tag{48}$$

Fig. 8 shows the previous range of slack (purple solid line – maximum, and green dashed line – minimum) in the absence of the tensioner. The tensioner action, which is the amount of slack taken up, is given by the blue dotted line. The new range of slack variation, as a result of the tensioner action, is given by the purple and green dash-dot lines. It can be observed that the tensioner action has been optimized so that it never exceeds the minimum slack curve of the transmission system (green dashed line) to avoid stretching the cable, which can theoretically cause over-constraint or jamming in the transmission. We took this conservative approach to the tensioner design because this was the first design iteration and several modeling assumptions (e.g. inextensible cables, decoupling of the end-effector actuation planes) had been made. Once a trend is established via experiments on how slack varies in the cable transmission system, without and with the tensioner, a more aggressive tensioner can be designed depending on the actual application.

Fig. 8 demonstrates the potential of the proposed tension management and slack mitigation solution. If the end-effector links were configured to be rotated by equal angles and there was no gap between the cables and the holes in the links, the tensioner designed above would result in an overall system slack given by the dash-dot green line. This shows a very low magnitude of slack variation over the range of actuation and the final value of slack at the maximum pulley angle goes to zero. This concludes the analysis and design of the proposed tensioning system. The next section discusses the experimental validation of the slack models and effectiveness of the tensioner.

4. Experimental validation

Now that the kinematic models for slack variation have been developed and the optimal geometric parameters of the tensioner have been determined, the slack estimate models along with the effectiveness of the tensioner geometry are experimentally validated. The experimental setup, seen in Fig. 9, consists of two actuation axes – Primary and Secondary – to articulate the end-effector in two orthogonal planes. The Primary axis is where we implement the proposed kinematic tensioner and conduct the relevant slack measurements with and without the

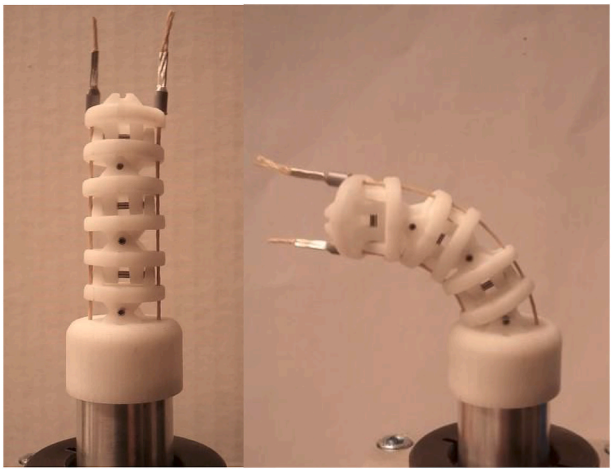

Fig. 10. Multi-link end-effector.

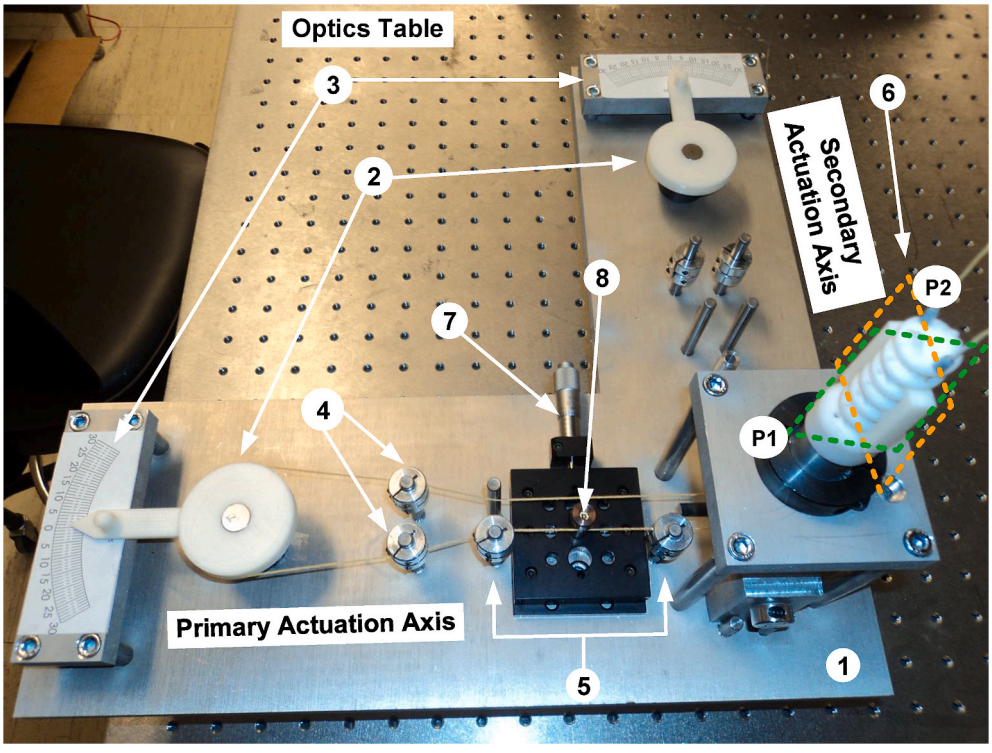

Fig. 9. Experimental setup.

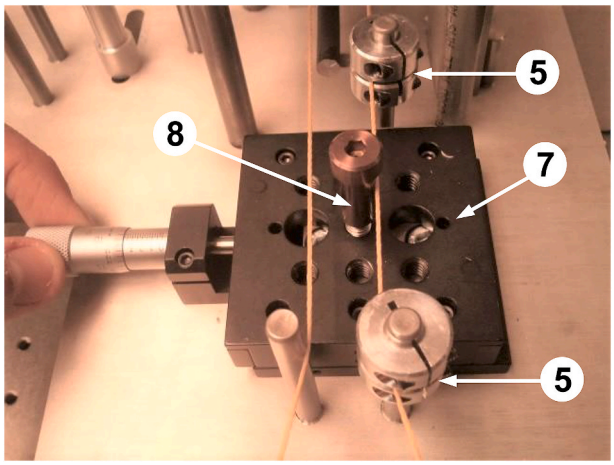

Fig. 11. Micrometer stage for slack measurement.

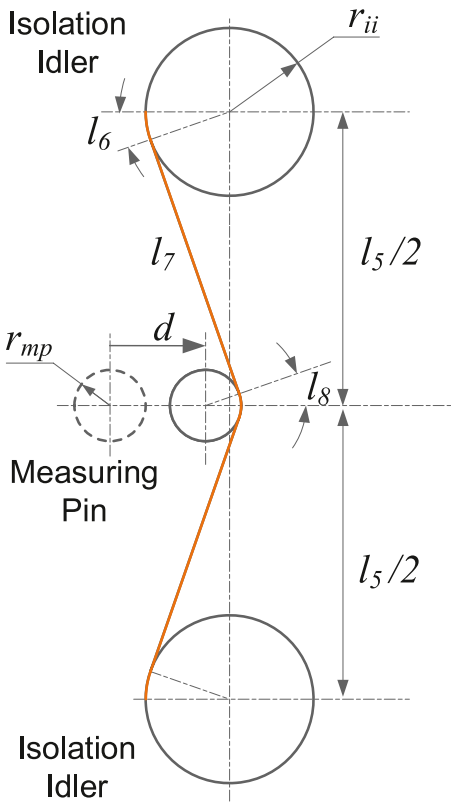

Fig. 12. Slack measurement scheme.

tensioner. The Secondary axis serves like a traditional cable transmission (e.g. Fig. 1a) to provide a baseline. All components are mounted on an aluminum base plate (1) that has been water-jet cut. The base plate itself is mounted to an Optics Table. The input pulleys (2) on each axis actuate the motion of the end-effector in their respective planes *P1* and *P2*. Each axis is equipped to measure the input pulley angle via respective measuring scales (3). The 3D-printed ABS input pulleys (2) consists of an extended indicator to help measure the input pulley angle (θ_p). The primary idlers (4) in conjunction with the isolation idlers (5) guide the cables appropriately to the end-effector (6). These idlers have been constructed by precisely mounting shaft collars onto dowel pins. The dowels are press-fit into the base plate and the lower shaft collar on each pin is mounted to the appropriate height above the base plate using gauge blocks. The upper shaft collar is mounted to accommodate the cable diameter to pass through the gap between the two collars, without altering the plane of the cable path. The isolation idlers (5) are used to isolate a section of the non-driving side cable in the overall cable transmission for the purpose of slack measurement. A micrometer stage (7), with a precision shoulder bolt (8) mounted on it, is used to measure slack in the cable at various input pulley angles. Finally, a roller assembly (not visible) underneath the end-effector is used to change the direction of the incoming cables, from horizontal to vertical, and attach them to the final link of the end-effector.

The end-effector, shown in the nominal and actuated conditions in Fig. 10, has also been 3D-printed and assembled. Spacers (not shown) are used to align the end-effector in its initial nominal condition, as no stiffness elements have been incoporated in the end-effector design to maintain its nomimal shape or to facilitate equal angle actuation.

4.1. Slack Measurement Scheme

A 5/16" diameter precision shoulder bolt mounted on the micrometer stage, configured to move normal to cable, is used to calculate slack in the non-driving side cable for a given input pulley angle, as shown in Fig. 11. The geometry of this measurement scheme can be seen in Fig. 12.

Slack is measured in the following manner:

i) The input pulley is rotated by a fixed increment using the measuring scale (1) and locked in place using a shaft clamp mounted at the bottom of the base plate. This causes the end-effector to articulate in one direction.

ii) The micrometer is slowly advanced. The shoulder bolt starts impinging into the non-driving side cable and picks up any existing slack. The micrometer is advanced till the end-effector wiggles slightly opposite to the direction of articulation. This signals that all the slack in the non-driving side cable has been picked up.

iii) The distance d is measured using the micrometer. Via the geometry of the measuring schemes, for known dimensions (in *inches*):$r_{ii} = 0.144$, $r_{mp} = 0.156$ and $l_5 = 3$, the slack in the cable can be determined.

$$Slack_{\exp} = 2(l_6 + l_7 + l_8) - l_5 \tag{51}$$

Relation (51) gives the experimentally measured slack in the system. Data measured from four experiments with no tensioner action is plotted in Fig. 13. The differences between the four experimental measurements are explained by the fact that the end-effector is under-actuated and therefore not fully deterministic. Nevertheless, some trends are clear. All the experimental slack measurements lies within the predicted range of slack variation (purple solid line – maximum, and green dashed line – minimum). This shows that the actual link rotations are somewhere between equal angle and step-wise actuation. Also, one can observe that the final slack in the system at the input pulley maximum angle of actuation is closer to the predicted maximum slack of the Realistic Model (RM). This indicates that at the maximum angle of the end-effector orientation, real effects indeed play a role and the cable axes tend to deviate from the hole axes in the links.

Now that the slack model has been validated, the efficacy of the tensioner design is tested. As stated in the previous section, optimization is performed with respect to the minimum predicted slack variation in the system to avoid any over-constraint in the transmission. Fig. 14 shows the modified input pulley with the tensioner extensions and pins incorporated. It consists of two flanges, an upper flange and a lower flange. Dowels are used as tensioner pins that are lightly press-fit into the holes on the flanges. The lower flange has a blind hole of a certain depth to seat the tensioner pin. The light press-fit enables easy removal of the pin. Multiple holes exist on the flange to accommodate the testing of multiple tensioner geometries.

Fig. 15 shows the theoretically predicted range of slack variation (purple dash-dot line – maximum, and green dash-dot line – minimum)

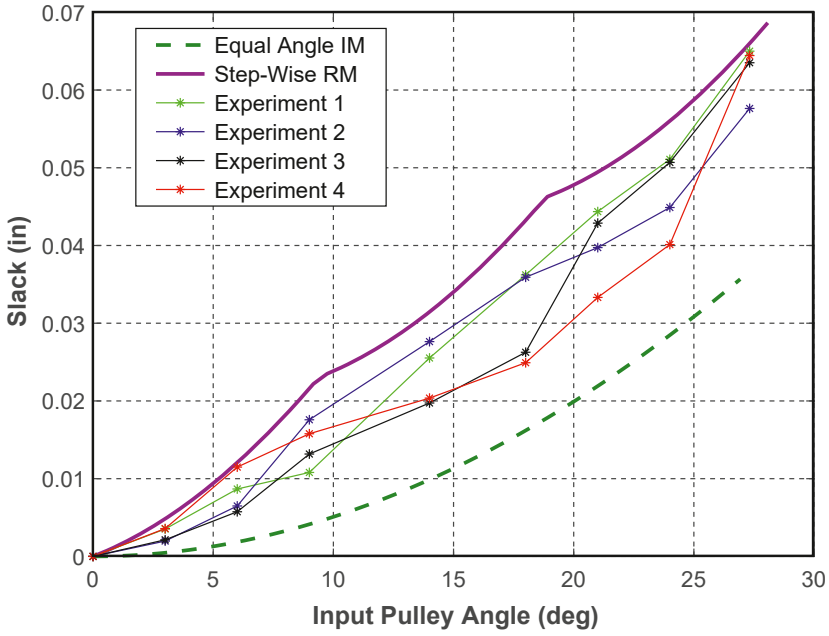

Fig. 13. Experimental slack measurements without tensioner.

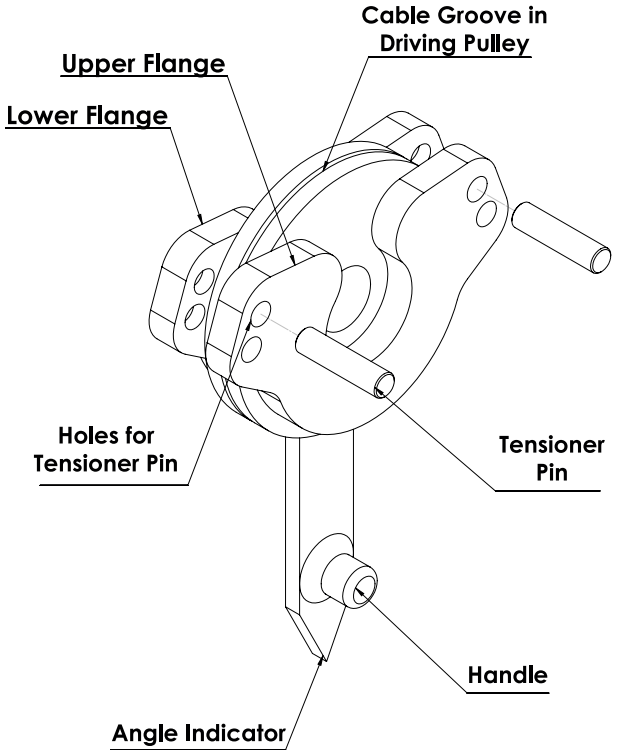

Fig. 14. Tensioner design.

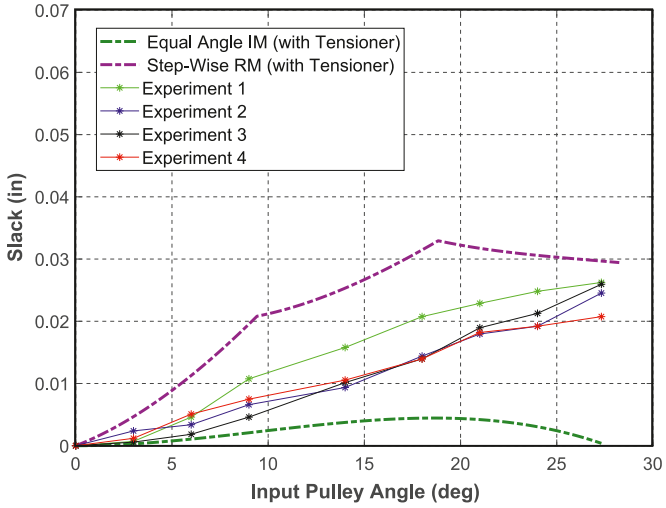

Fig. 15. Experimental slack measurement with tensioner.

with the tensioner action. The four experimental measurements of slack variation with input pulley rotation in the presence of tensioner action are within the expected bounds predicted by the model. The experimental measurements also suggest that the actual link rotations are somewhere between equal angle and step-wise actuation. As before, the maximum experimentally measured slack is closer to the Realistic Model (RM) prediction, particularly at the maximum angle of input pulley actuation and end-effector orientation. This highlights the role of real effects, i.e., the cable diameter slightly less than the hole diameter. If the cable diameter was exactly equal to the hole diameter, then with this particular tensioner, it would be possible to significantly lower the slack over the course of actuation and it would be possible to achieve close to zero slack at the maximum angle of actuation. Furthermore, if the end-effector links were constrained to rotate by equal angles, then the remaining slack in the presence of tensioner action would be close to zero over the entire range of actuation.

In the current setup, a comparison of the experimental slack data in Figs. 13 and 15 shows that slack has been reduced almost by half. In fact, for input angles greater than 10°, the worst case slack with the tensioning system is still better than the best case slack without the tensioning system incorporated into the transmission. Also, this was merely the first design iteration. These results show that tensioner action can be designed to be more aggressive to take up further slack in the

presence of real effects such as gap between cables and respective holes as well as compliance of the cables.

5. Conclusion

This paper highlights the problem of slack in cable transmissions systems and provides a review of limitations and tradeoffs associated with existing slack mitigation solutions. Using the example of a remote multi-link end-effector, we present an analytical formulation for the kinematic component of slack generated in the non-driving side of the cable transmission. We propose a novel tensioning system that effectively mitigates slack via a simple modification to the driving pulley in the form of rigid tensioner extensions that alter the cable path on the non-driving side of the cable transmission during actuation. This arrangement kinematically picks up the slack on the non-driving side cable, while avoiding the limitations and tradeoffs associated with previous solutions. The analytical formulation of kinematic slack is used to predict the range of slack variation with input pulley angle under various conditions (e.g. equal angle versus step-wise actuation, and ideal versus realistic models). Similarly, an analytical formulation is provided for the slack picked up the proposed tensioning system. These analytical formulations for slack generation and slack pick up are then used to optimally design the dimensions of the tensioner to minimize slack in an actual multi-link end effector that articulates in two orthogonal planes. The slack predictions without and with the proposed tensioner are then successfully validated using an experimental setup. The experimental measurements validate the efficacy of the proposed solution in reducing slack in the cable transmission without causing jamming or over-constraint. The models presented here and the proposed solution are easily scalable and can be readily used in a wide range of applications that employ cable transmission for bidirectional actuation of an end-effector using a single drive pulley with finite input rotation.

Although the focus of this paper was on modeling and mitigating the kinematic component of slack, the proposed tensioner concept is equally effective for elastic component of slack as well. The latter can be modeled and incorporated into the optimization routine to synthesize a suitable tensioner. Also, while one embodiment of the proposed tensioner design was developed, fabricated, and tested here, there exist several alternate embodiments and variations [2]. Future work involves modeling and testing these variations.

Declaration of competing interest

The subject of this paper is captured in the patent application:

Tension Management Apparatus for Cable-driven Transmission, US Patent Application 15/564,112 [2].

This patent application is licensed to FlexDex Surgical that sells a commercial product that incorporates the novel design described in this paper. Author Shorya Awtar has a financial interest in FlexDex Surgical.

References

[1] Hegeman, D.A., Danitz, D.J., Bertsch, K.S., Alvord, L.J., and Hinman, C.D., 2011, “Articulating tool with improved tension management system”, US Patent 7,862,554 B2.

[2] Awtar, S., 2016, “Tension management apparatus for cable-driven transmission”, US Patent Application 15/564,112.

[3] Awtar, S., Nielsen, J., Trutna, T., Mansfield, A., Abani, R., Geiger, J., and Quigley, P., 2014, “Minimal access tool”, US Patent 8,668,702 B2.

[4] Van Meer F, Giraud A, Esteve D, Dollat X. A disposable plastic compact wrist for smart minimally invasive surgical tools. In: *2005* IEEE/RSJ International conference on Intelligent robots and systems; 2005. p. 919–24. https://doi.org/10.1109/IROS.2005.1545440.

[5] Peirs J, Van Brussel H, Reynaerts D, De Gersem G. A flexible distal tip with two degrees of freedom for enhanced dexterity in endoscopic robot surgery. In: MME'02, the 13th micromechanics Europe Workshop, October 6-8, 2002, Sinaia, Romania; 2002.

[6] Jinno M, Matsuhira N, Sunaoshi T, Hato T, Miyagawa T, Morikawa Y, Furukawa T, Ozawa S, Kitajima M, Nakazawa K. Development of a master slave combined manipulator for laparoscopic surgery: functional model and its evaluation. In: Dohi T, Kikinis R, editors. Medical image computing and computer-assisted intervention - MICCAI 2002. Lecture notes in computer science, vol. 2488. Berlin, Heidelberg: Springer; 2002. p. 52–9. https://doi.org/10.1007/3-540-45786-0_7.

[7] Omori, S., Uenohara, S., Jinno, M., and Sunaoshi, T., 2008, “Manipulator”, US Patent Application 11/870,849.

[8] Cooper, T.G., Wallace, D.T., Chang, S., Anderson, S.C., Williams, D., and, Manzo, S., 2004, “Surgical tool having positively positionable tendon-actuated multi-disk wrist joint”, US Patent 6,817,974 B2.

[9] Do TN, Tjahjowidodo T, Lau MWS, Phee SJ. Adaptive control of position compensation for cable-conduit mechanisms used in flexible surgical robots. In: *2014 11th International Conference on Informatics in control*, automation and robotics (ICINCO); 2014. p. 110–7. https://doi.org/10.5220/0005114701100117.

[10] Liang Y, Du Z, Wang W, Sun L. A novel position compensation scheme for cable-pulley mechanisms used in laparoscopic surgical robots. Sensors 2017;17(10): 2257. https://doi.org/10.3390/s17102257.

[11] Wang W, Yu L, Yang J. Toward force detection of a cable-driven micromanipulator for a surgical robot based on disturbance observer. Mechanical Sciences 2017;8: 323–35. https://doi.org/10.5194/ms-8-323-2017.

[12] Walker ID, Hannan MW. A novel ‘elephant’s trunk’ robot. In: 1999 IEEE/ASME International conference on advanced Intelligent mechatronics; 1999. p. 410–5. https://doi.org/10.1109/AIM.1999.803204.

[13] Li C, Rahn CD. Design of continuous backbone, cable-driven robots. ASME Journal of Mechanical Design 2002;124(2):265–71. https://doi.org/10.1115/1.1447546.

[14] Immega G, Antonelli K. The KSI tentacle manipulator. In: Proceedings of 1995 IEEE international conference on robotics and automation, Nagoya, Japan, vol. 3; 1995. p. 3149–54. https://doi.org/10.1109/ROBOT.1995.525733.

[15] Jacobsen SC, Ko H, Iversen EK, Davis CC. Antagonistic control of a tendon driven manipulator. In: Proceedings, 1989 international conference on robotics and automation, vol. 3; 1989. p. 1334–9. https://doi.org/10.1109/ROBOT.1989.100165.

[16] Shirafuji S, Ikemoto S, Hosoda K. Development of a tendon-driven robotic finger for an anthropomorphic robotic hand. Int J Robot Res 2014;33(5):677–93. https://doi.org/10.1177/0278364913518357.

[17] Borghesan G, Palli G, Melchiorri C. Design of tendon-driven robotic fingers: modeling and control issues. In: *2010* IEEE International conference on robotics and automation; 2010. p. 793–8. https://doi.org/10.1109/ROBOT.2010.5509899.

[18] Inouye JM, Valero-Cuevas FJ. Anthropomorphic tendon-driven robotic hands can exceed human grasping capabilities following optimization. Int. J. Robot. Res. 2013;33(5):694–705. https://doi.org/10.1177/0278364913504247.

[19] Li C, Gu X, Ren H. A cable-driven flexible robotic grasper with Lego-like modular and reconfigurable joints. IEEE ASME Trans Mechatron 2017;22(6):2757–67. https://doi.org/10.1109/TMECH.2017.2765081.

[20] Grosu S, De Rijcke L, Grosu V, Geeroms J, Vanderboght B, Lefeber D, Rodriguez-Guerrero C. Driving robotic exoskeletons using cable-based transmissions: a qualitative analysis and overview. ASME Applied Mechanics 2018;70(6):16. https://doi.org/10.1115/1.4042399. 060801.

[21] Cable-driven parallel robots. In: Pott A, Bruckmann T, editors. Proceedings of the 4th International conference on cable-driven parallel robots (CableCon 2019). Springer; 2019. https://www.springer.com/gp/book/9783030207502.

[22] Oh So-Ryeok, Agrawal SK. Cable suspended planar robots with redundant cables: controllers with positive tensions. IEEE Trans Robot 2005;21(3):457–65. https://doi.org/10.1109/TRO.2004.838029.

[23] Chang, Y.-J., Chou, K.-T., Chen, T.-C., and Chen, C.-Y., 2018, “Steel wire transmission system for three-dimensional printer and adjusting mechanism thereof”, US Patent 10,065,372.

[24] Pigford, J.D., 1957, “Cable quadrant assembly”, US Patent 2,810,300.

[25] Wrighton RJ. Cable tension regulator. US Patent 1957;2(866):355.

[26] Amato F, Carbone M, Cosentino C, Merola A, Morelli M, Zullo F. A versatile mechatronic tool for minimally invasive surgery. In: The first IEEE/RAS-EMBS International conference on biomedical robotics and biomechatronics, 2006. BioRob 2006., Pisa; 2006. p. 192–7. https://doi.org/10.1109/BIOROB.2006.1639083.

[27] Marco F, Antonio F, Fabio S, Massimo B. Kinematics of a new 2-DoF wrist with high angulation capability. IEEE International Conference on Robotics and Automation (ICRA 2006:1524–9. https://doi.org/10.1109/ROBOT.2006.1641924.

[28] Minor M, Mukherjee R. A dexterous manipulator for minimally invasive surgery. In: 1999 IEEE International conference on robotics and automation, Detroit, MI, USA. vol. 3; 1999. p. 2057–64. https://doi.org/10.1109/ROBOT.1999.770410.

[29] C. Ishii, K. Kobayashi, Y. Kamei and Y. Nishitani, "Robotic forceps manipulator with a novel bending mechanism," IEEE ASME Trans Mechatron, vol. 15(5), pp. 671-684, doi: 10.1109/TMECH.2009.2031641.

[30] Yamashita H, Hata N, Hashizume M, Dohi T. Handheld laparoscopic forceps manipulator using multi-slider linkage mechanisms. In: Barillot C, Haynor DR, Hellier P, editors. Medical image computing and computer-assisted Intervention – MICCAI 2004; 2004.

[31] Maguire, J.M. and Deneszczuk, W.C., 2011, “Drive belt tensioner for motor generator unit”, US Patent Application 12/562,524.